LDV measurements of Unsteady Blade Suction-Surface Flow of an Axial-Flow Turbine Rotor

Takayuki Matsunuma

National Institute of Advanced Industrial Science and Technology (AIST)
1-2-1 Namiki, Tsukuba, Ibaraki, 305-8564, Japan

ABSTRACT

The unsteady flow field of an axial-flow turbine rotor was investigated experimentally using a laser Doppler velocimetry (LDV) system. Detailed measurements of the time-averaged and time-resolved distributions of the velocity, flow angle, turbulence intensity, etc. were carried out at a low Reynolds number condition, $Re_{out,RT} = 3.5 \times 10^4$. The data obtained were analyzed from the viewpoints of both an absolute (stationary) frame of reference and a relative (rotating) frame of reference. The effect of the turbine nozzle wake and secondary vortices on the rotor flow field was clearly captured. It was found that the nozzle wake and secondary vortices are suddenly distorted at the rotor inlet, because of the rotating potential field of the rotor. The nozzle flow (wake and secondary vortices) and the rotor surface flow (boundary layer flow) interact intensively inside the rotor passage. The periodic fluctuation of the relative velocity on the rotor suction surface due to the nozzle effect is as much as 20% of the mean rotor exit velocity.

Key Words: LDV measurement, Axial-flow turbine, Rotor, Unsteady flow, Wake, Secondary vortex

1. Introduction

The flow field around turbine blades is very unsteady and complex due to "rotor-stator interaction," the aerodynamic interaction between the turbine nozzle (stator) and the turbine rotor. Boundary layer behavior, loss generation, secondary vortex growth, and heat transfer in turbines are strongly affected by the rotor-stator interaction. Even though unsteady flow plays an important role in axial-flow turbines, turbines are mainly designed using steady-flow calculations. Because few actual models exist for the loss-generating mechanisms seen in unsteady flow, empirical correlations are used to account for the effects of unsteadiness. Therefore, more knowledge on unsteady rotor-stator interaction is essential to increase the performance of turbines. Although a variety of measurement techniques can easily be applied to the flow field within the stationary blades, difficulties arise with measurements of the flow field within the rotating blades. Binder et al. [1], Zaccaria and Lakshminarayana [2], Göttlich et al. [3], and Matsunuma [4] used laser measurement systems, such as laser two-focus velocimetry (L2F), laser Doppler velocimetry (LDV), and particle image velocimetry (PIV).

This paper focuses on the unsteady effect of turbine nozzle wake and secondary vortices (passage vortex and trailing edge vortex) on the suction surface flow of an axial-flow turbine rotor.

2. Experimental Facility and Method

2.1 Annular turbine wind tunnel and turbine cascade

Figure 1 shows the annular turbine wind tunnel used in the experiment. This wind tunnel is an air suction type, open circuit facility. The total length of the wind tunnel is approximately 3.8 meters. The outside and inside annular wall diameters of the test section are 500 mm and 350 mm, respectively. A single-stage axial-flow turbine designed using a free vortex method to attain radial equilibrium was installed at the test section. The geometries and specifications of the turbine nozzle and rotor cascades are shown in Fig. 2, Fig. 3, and Table 1.
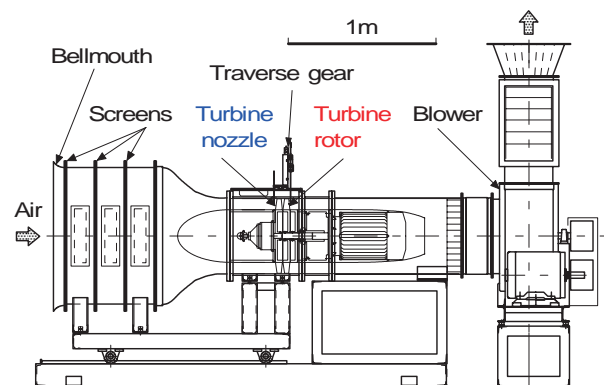
Figure 1   Annular turbine wind tunnel

(a) Tip   (b) Midspan   (c) Hub
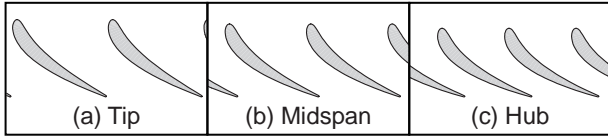
Figure 2   Geometry of turbine nozzle

(a) Tip   (b) Midspan   (c) Hub
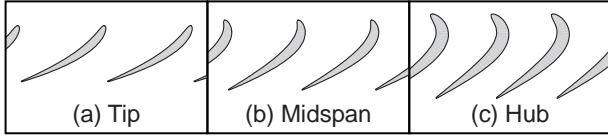
Figure 3   Geometry of turbine rotor

Table 1   Specifications of turbine cascades

	Nozzle			Rotor		
	Tip	Mid	Hub	Tip	Mid	Hub
		28			31	
Chord, C mm	69.1	67.6	66.1	58.5	58.5	58.5
Axial chord, C_{ax} mm	45.0	42.5	40.0	32.3	40.9	48.0
Blade span, H mm		75.0			74.0	
Blade pitch, S mm	56.1	47.7	39.3	50.7	43.1	35.5
Aspect ratio, H/C	1.09	1.10	1.13	1.26	1.26	1.26
Solidity, C/S	1.23	1.42	1.68	1.15	1.42	1.65
Inlet flow angle, α_1 deg	0.0	0.0	0.0	-16.5	21.8	51.7
Exit flow angle, α_2 deg	63.9	67.4	71.1	66.9	63.4	58.7
Stagger angle, ξ deg	49.3	51.0	52.7	55.9	47.6	33.4
Inner diameter, D_1 mm		350			350	
Outer diameter, D_2 mm		500			500	
Hub/tip ratio, D_1/D_2		0.7			0.7	
Tip clearance, τ mm		0.0			1.0	

2.2 LDV measurement system and data analysis method

A photograph of the wind tunnel and the LDV measurement system is shown in Fig. 4. The LDV system was a standard two-color, four-beam, two-dimensional measuring system with a fiber-optic probe (System 90-3, TSI Inc.). The system consisted of a 4 W argon-ion laser tuned to 488 nm (blue) and 514.5 nm (green) output. The fiber-optic probe was mounted on a three-dimensional traverse gear. The half-angle between the beams was 4.29 deg. and the calculated dimensions of the measurement volume at e^{-2} intensity locations were 0.85 mm in length and 0.073 mm in diameter. Dantec Safex standard fog fluid with a mean particle diameter of 1.068 μm was used to seed the flow. The liquid was atomized using a Dantec Safex Model 2001 fog generator. Tracer particles were introduced into the test section from the wind tunnel inlet. An incremental rotary encoder (1,800 pulses/revolution) was attached to the rotor shaft to detect the rotor angular position. An automatic measurement system controlled by a personal computer was adopted in this study, and all measured data were stored on a hard disk in the computer.
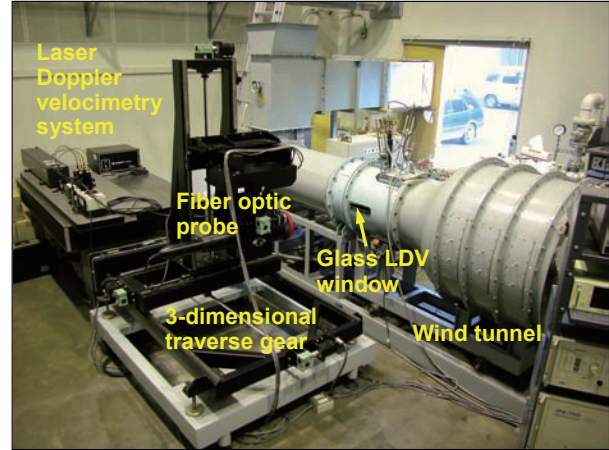
Figure 4   Wind tunnel and LDV system
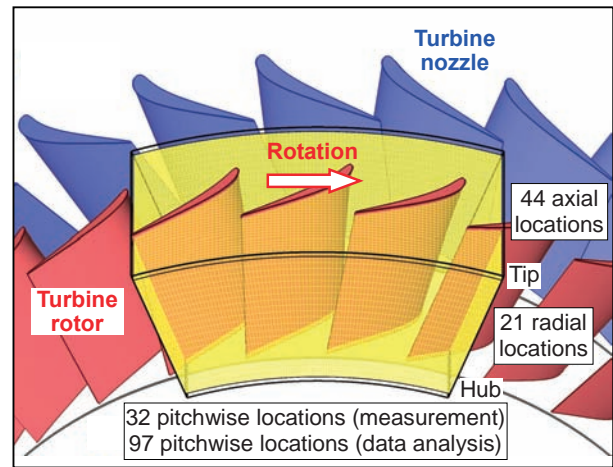
Figure 5   LDV measurement locations

Figure 5 shows the LDV measurement locations around the rotor. Measurements were taken at 44 axial locations from immediately downstream of the nozzle to downstream of the rotor (an axial interval of 2 mm), 21 spanwise locations (from 3.3% span to 96.7% span), and 32 pitchwise locations for one pitch of the nozzle. Ninety-seven pitchwise data (three nozzle pitches) were displayed in the subsequent data analysis to make the flow clearly intelligible. Since two-dimensional LDV was applied, the axial and circumferential velocities (V_Z and V_X) were measured. At each measurement point, 10,000 instantaneous velocity samples were collected. Ensemble averaging of the instantaneous velocity data was performed with the help of the rotor encoder signal. The relative velocity V_{Rel} and turbulence intensities Tu_{Rel} were calculated as follows:

$$V_{Rel} = \sqrt{V_Z^2 + (V_{X,Abs} + V_{RT})^2} \Big/ V_2$$

$$Tu_{Rel} = \sqrt{\frac{v_z'^2 + v_x'^2}{2}} \Big/ V_2$$

All data presented in this paper are nondimensional. The time-averaged, pitchwise-averaged, and spanwise- averaged relative velocity

V_2 at the rotor exit (V_2 = 9.27 m/s) made the velocity and turbulence intensity in the relative frame of reference dimensionless.

It should be noted that this paper describes rotor synchronous unsteady effects because the ensemble averaging purges all nonrotational effects, such as instabilities, trailing edge vortex shedding, etc.

The Reynolds number used during the experiment was set at $Re_{in,NZ}$ = 2.0 x 10^4 based on the nozzle chord length and nozzle inlet velocity. The reason for using the Reynolds number of the nozzle inlet $Re_{in,NZ}$ was because the flow condition at the nozzle inlet is easy to measure. The Reynolds number based on the rotor chord length and rotor exit velocity $Re_{out,RT}$ was calculated as 3.5 x 10^4 from the measured LDV data. The axial velocity at the test section was 4.47 m/s and the rotor speed was set at 402 rpm to attain the design operating condition (design rotor inlet flow

angle). The flow in this experiment was considered to be incompressible because the Mach number was very low. The Mach numbers based on the mass-averaged velocities at the nozzle inlet, nozzle outlet, rotor inlet, and rotor outlet were $M_{in,NZ}$ = 0.013, $M_{out,NZ}$ = 0.031, $M_{in,RT}$ = 0.014, and $M_{out,RT}$ = 0.027, respectively. The author would like to note that the flow in actual gas turbines should be considered compressible because those Mach numbers are typically M_{out} = 0.5 to 1.2.

3. Results and Discussion

Figure 6 shows the time-averaged flow close to the rotor suction surface. Figures 6(a) and 6(b) show the relative velocity and the turbulence intensity, respectively. The main flow moves from right to left as indicated by the light green arrows in these figures. In Fig. 6(a), a large boundary layer region associated with the low relative velocity was observed at the rear section of the suction surface. This is because the thickness of the boundary layer developed from the rotor leading edge increases rapidly at the adverse pressure gradient region on the rear part of the suction surface. The existence of flow separation on the suction surface could not be confirmed from the LDV measurements because of insufficient measurement resolution in the boundary layer region. The pink solid line in the figure indicates the thick boundary layer onset line, which was defined as the position with the maximum velocity gradient (largest decrease in velocity). Low relative velocity regions due to the rotor tip leakage and passage vortex are observed near the tip and hub endwalls. In Fig. 6(b),

(a) Relative velocity   (b) Turbulence intensity
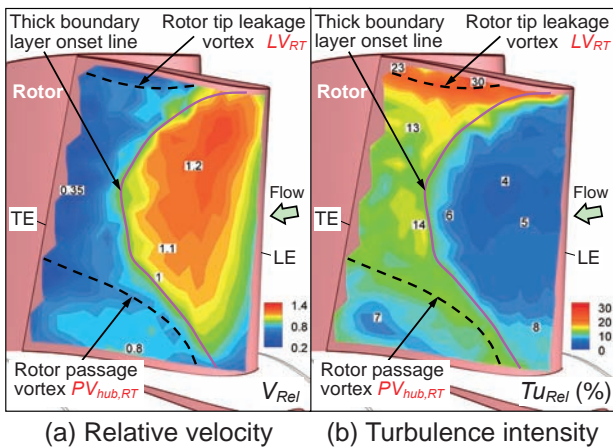
Figure 6   Time-averaged flow on rotor suction surface
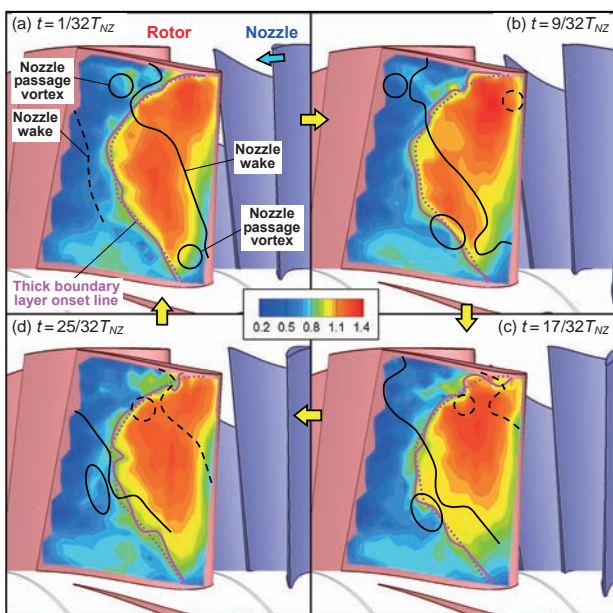
Figure 7   Time-resolved relative velocity on rotor suction surface
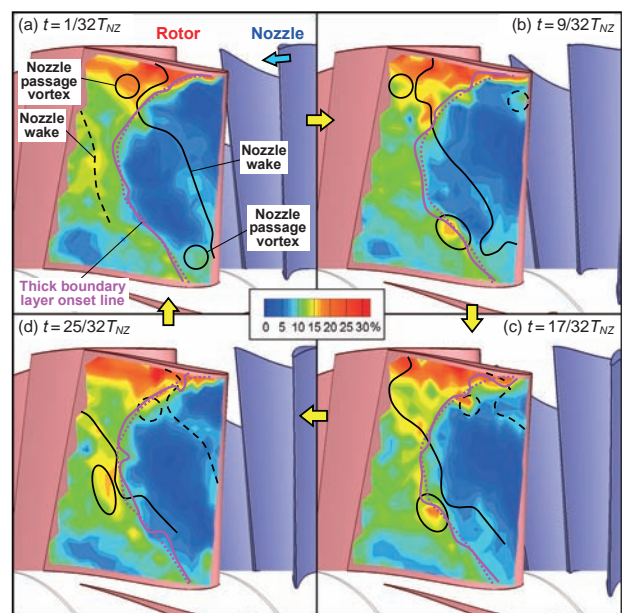
Figure 8   Time-resolved turbulence intensity on rotor suction surface
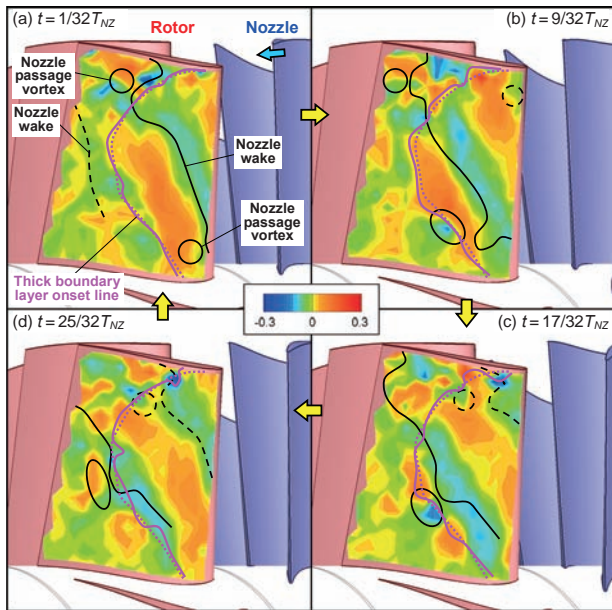
Figure 9 Periodic fluctuation of time-resolved relative velocity on rotor suction surface

Figure 10 Periodic fluctuation of time-resolved turbulence intensity on rotor suction surface

the turbulence intensity increases dramatically behind the thick boundary layer onset line. The tip leakage vortex generates a high turbulence intensity region near the tip endwall. The maximum value of the turbulence at the tip leakage vortex region is approximately 30%.

Figures 7 and 8 show the time-resolved relative velocity and turbulence intensity close to the rotor suction surface, respectively. Figures 9 and 10 show the periodic fluctuations of the time-resolved relative velocity and turbulence intensity close to the rotor suction surface, respectively. The periodic fluctuations were obtained by subtracting the time-averaged distributions in Fig. 6 from the time-resolved distributions in Figs. 7 and 8. The pink solid lines in these figures indicate the time-resolved thick boundary layer onset lines. In order to observe the unsteady motion of the lines, the time-averaged thick boundary layer onset line in Fig. 6 is superimposed on the figures, as indicated by the pink dotted lines. The approximate positions of the nozzle wake and the nozzle passage vortices are shown by the black lines and circles in the figures. The black line was defined as the high turbulence intensity position due to the nozzle wake and passage vortices. The nozzle wake and passage vortices generate large fluctuations of the relative velocity and turbulence intensity on the rotor suction surface. The range of periodical fluctuation of the relative velocity due to the nozzle effect is about 20% of the mean exit velocity V_2. The nozzle wake and passage vortices also have a moderate effect on the boundary layer

region. The interaction between the rotor boundary layer flow and the nozzle wake and passage vortices generates complex local skews on the thick boundary layer onset line. It is evident that the thick boundary layer onset line locally moves upstream under the effect of the nozzle wake.

4. Summary

Laser Doppler velocimetry (LDV) was successfully applied to provide detailed experimental data on the time-resolved unsteady flow fields around the rotor of a single-stage axial-flow turbine at a low Reynolds number ($Re_{out,RT} = 3.5 \times 10^4$). The complex aerodynamic interactions between the turbine nozzle and the turbine rotor were described in detail. The periodic fluctuation of the relative velocity on the rotor suction surface due to the nozzle effect is as much as 20% of the mean rotor exit velocity. The nozzle wake and passage vortices generate complex local skews of the thick boundary layer onset line.

References

[1] Binder, A., Forster, W., Mach, K., and Rogge, H., 1987, ASME *J. of Turbomachinery*, Vol. 109, pp. 251–257.

[2] Zaccaria, M. A., and Lakshminarayana, B., 1995, ASME *J. of Turbomachinery*, Vol. 119, pp. 201–224.

[3] Göttlich, E., et al.Woisetschläger, J., Pieringer, P., Hampel, B., and Heitmeir, F., 2006, ASME *J. of Turbomachinery*, Vol. 128, pp. 178–187.

[4] Matsunuma, T., 2007, ASME *J. of Turbomachinery*, Vol. 129, pp. 360–371.